Journal of Alloys and Compounds 509 (2011) 837–844

Contents lists available at ScienceDirect

Journal of Alloys and Compounds

journal homepage: www.elsevier.com/locate/jallcom

Sol–gel preparation and characterization of uniform core-shell structured $LaInO_3:Sm^{3+}/Tb^{3+}@SiO_2$ phosphors

Yongchen Shang[a], Piaoping Yang[b,*], Wenxin Wang[b], Yanli Wang[b], Na Niu[b], Shili Gai[b], Jun Lin[c,*]

[a] College of Chemistry, Harbin Normal University, Harbin 150025, PR China
[b] College of Material Science and Chemical Engineering, Harbin Engineering University, 145 Nantong Street, Harbin 150001, PR China
[c] State Key Laboratory of Rare Earth Resource Utilization, Changchun Institute of Applied Chemistry, Chinese Academy of Sciences, Changchun 130022, PR China

ARTICLE INFO

Article history:
Received 12 July 2010
Received in revised form
16 September 2010
Accepted 18 September 2010
Available online 25 September 2010

Keywords:
Core-shell
$LaInO_3$
Luminescence
Phosphors
Sol–gel synthesis

ABSTRACT

The core-shell structured $LaInO_3:Ln^{3+}@SiO_2$ ($Ln^{3+} = Sm^{3+}$, Tb^{3+}) phosphors were realized by coating $LaInO_3:Ln^{3+}$ phosphors on the surface of silica microspheres via a modified Pechini sol–gel process. The phase, structure, morphology, and fluorescent properties of the materials were well characterized by means of X-ray diffraction (XRD), field emission scanning electron microscopy (FE-SEM), transmission electron microscopy (TEM), Fourier transform IR spectroscopy (FT-IR), photoluminescence (PL) spectra, cathodoluminescence (CL) spectra, and the kinetic decays, respectively. The results reveal that the obtained core-shell structured phosphors consist of amorphous silica core and crystalline $LaInO_3:Ln^{3+}$ shell, which keep the uniform spherical morphology of pure silica spheres with narrow size distribution. Upon excitation by ultraviolet (UV) irradiation or electron beam, the phosphors show the characteristic emission lines of Sm^{3+} ($^4G_{5/2}$–$^6H_{5/2,7/2,9/2}$, orange) in $LaInO_3:Sm^{3+}@SiO_2$ and characteristic emissions of Tb^{3+} ($^5D_4$–$^7F_{6,5,4,3}$, green) in $LaInO_3:Tb^{3+}@SiO_2$, respectively. This kind of phosphors may have potential applications in field emission displays (FEDs) based on their uniform shape, low-cost synthetic route, and diverse luminescent properties.

1. Introduction

During the past decades, doping has been extensively applied for the fabrication of hybrid materials with desirable properties and functions in modern materials science and engineering [1–10]. For rare earth based luminescent materials, doping is of fundamental importance in achieving and modifying the optical properties due to their abundant emission colors based on their unique 4f–4f or 4f–5d transitions [11–15]. The 4f emission spectra of rare earth ions are characterized by narrow lines with high color purity due to the shielding of 4f electrons by outer 5s and 5p electrons [11]. Furthermore, the host lattice has little influence on the positions of the 4f configuration energy levels, which are almost the same as the free-ion levels. These special properties are widely employed to develop novel fluorescent materials with narrow emission lines, which exhibit potential applications in the fields of luminescent devices, optical transmission, biochemical probes, and medical diagnostics [16–20].

Recently, the core-shell structured materials are of special interest due to their potential applications in various fields, such as diagnostics, catalysis, photonic crystals, and water treatment [21–25]. The structure, size and composition of these core-shell structured materials can be tuned in a controllable manner to tailor their functions [26–29]. Core-shell structured particles can preserve the magnetic, optical, and electronic properties of their corresponding core and/or shell components. Particularly, they can dramatically lower the cost of precious materials by coating them on inexpensive cores [30,31]. Up to now, diverse routes have been developed for the preparation of the core-shell structured materials, such as co-precipitation, layer-by-layer technique, template directed self-assembly, sol–gel process and MOCVD [32–36]. However, in most cases, the uniformity of the coating layer (shell) is low and it is difficult to control the shape and size of the final products. Among all the synthesis methods, a modified Pechini sol–gel process has been proved an efficient methodology to coat uniform crystalline thin film on the surface of silica spheres, using inorganic salt as precursor, citric acid as chelating agents, and poly (ethylene glycol) (PEG) as cross-linking ligands [37–42].

As a narrow-band (3.2 eV) semiconductor, $LaInO_3$ belongs to the perovskite structure in *Pnma* space group with some orthorhombic distortion [43]. The structure is composed of three dimensional sub-lattices with corner connected InO_6 octahedra and the La^{3+} is coordinated by eight-fold oxide ions. All the octahedra share their corners and are slightly tilted. Due to the narrow band, semiconducting $LaInO_3$ compounds may find potential applications as a

* Corresponding authors. Tel.: +86 451 82569890; fax: +86 431 85698401.
E-mail addresses: piaoping@ciac.jl.cn (P. Yang), jlin@ciac.jl.cn (J. Lin).

0925-8388/$ – see front matter © 2010 Elsevier B.V. All rights reserved.
doi:10.1016/j.jallcom.2010.09.105

host lattice for field emission displays (FEDs) [44–46]. Apart from the potential use in fluorescent field, bulk $LaInO_3$ crystals have also attracted much attention as one kind of electrolyte materials for solid fuel cells [47]. Rare-earth doped $LaInO_3$ phosphors have been reported in our group as an alternative FEDs material due to their higher thermal and chemical stabilities than those of the conventional sulfide-based phosphors [44,45]. However, the precious precursor materials (In_2O_3, La_2O_3, and rare earth oxides) result in the high cost of this kind of phosphors. Moreover, high performance in displaying applications requires the phosphors possess some unique features, such as suitable particle size, ideally spherical shape, and narrow size distribution. Therefore, the design of core-shell structured phosphors with these special properties should be highly promising. Up to data, little information on the core-shell structured materials related with the rare earth doped $LaInO_3$ phosphors has been reported. Herein, we proposed the fabrication of uniform core-shell structured $LaInO_3$:Ln^{3+}@SiO_2 microspheres via a facile and large-scaled Pechini sol–gel process by functionalization of silica spheres with fluorescent $LaInO_3$:Ln^{3+} layer. The physicochemical properties of the as-prepared samples were well examined by means of XRD, SEM, TEM, FT-IR, and luminescent spectra. A possible formation scheme is presented as well.

2. Experimental details

2.1. Preparation of monodisperse silica microspheres

Monodisperse silica microspheres with mean diameter of 300 nm were prepared via a modified Stöber process [48] by hydrolysis of TEOS in a mixed solution of alcohol, water and ammonia. A colloidal solution of silica particles in sub-micrometer range with narrow size distribution was obtained, while the particle sizes of silica depend on the relative concentrations of the reactants. In a typical process, the mixture containing tetraethyl orthosilicate (TEOS, 99%, Beijing Fine Chemical Company, China), H_2O, NH_4OH (A.R., Beijing Fine Chemical Company, China), and C_2H_5OH (A.R., Beijing Fine Chemical Company, China) with the concentration ratio of 0.17:7.5:1.0 was stirred at room temperature for 4 h, resulting in the formation of white silica colloidal suspension. The colloidal suspension was centrifugally separated from the suspension and washed with ethanol four times.

2.2. Preparation of $LaInO_3$:Ln^{3+}@SiO_2 microspheres

Deposition of $LaInO_3$:Ln^{3+} phosphors layer onto the surface of silica spheres was prepared by a modified Pechini sol–gel process [49]. The doping concentration of Sm^{3+} was 2 mol% of La^{3+} in $LaInO_3$:Sm^{3+} and Tb^{3+} was 5 mol% of La^{3+} in $LaInO_3$:Tb^{3+}, which had been optimized in our previous work [44]. In a typical route for the preparation of $LaInO_3$:Sm^{3+}@SiO_2, stoichiometric weights of In_2O_3 (A.R., Beijing Fine Chemical Company, China), La_2O_3 and Sm_2O_3 (99.99%, Science and Technology Parent Company of Changchun Institute of Applied Chemistry, China) were dissolved in dilute HNO_3 (A.R., Beijing Fine Chemical Company, China) with stirring. The superfluous HNO_3 was driven off by heating until the pH value of the solution reached between two and three, resulting in the formation of the colorless mixed solutions of $In(NO_3)_3$, $La(NO_3)_3$ and $Sm(NO_3)_3$. Then citric acid (A.R., Beijing Fine Chemical Company, China) with a molar ratio of 2:1 to rare earth ions was added as a chelating agent. Subsequently, polyethylene glycol (PEG, M_w = 10000) was added as a cross-linking agent with a concentration of 0.01 M. The mixture was stirred for 1 h. Then desired amount of as-prepared silica powder was added into the sol under stirring. The suspension was further stirred for another 3 h, then the resulting material was separated by centrifugation. The obtained product was condensed at 75 °C in a water bath until milky powder was formed. After being dried at 110 °C for 10 h, the powder was ground and treated at 450 °C for 4 h in air. Then the samples were fully ground and heated from room temperature to 900 °C with a heating rate of 1 °C/min and maintained at this temperature for 3 h in air. The coating process was repeated for three times. The final obtained product was designated as $LaInO_3$:Sm^{3+}@SiO_2. $LaInO_3$:Tb^{3+}@SiO_2 was prepared in a much similar process except for the doping Sm^{3+} (2%) has been replaced by Tb^{3+} (5%). Furthermore, after being pre-treated at 450 °C for 4 h in air, the sample was fully ground and heated from room temperature to 900 °C with a heating rate of 1 °C/min and maintained at this temperature for 3 h in the mixture of hydrogen and nitrogen to produce the final sample. In this way, the luminescent $LaInO_3$:Tb^{3+} coated silica spheres were obtained (denoted as $LaInO_3$:Tb^{3+}@SiO_2). The formation process of core-shell structured $LaInO_3$:Sm^{3+}@SiO_2 phosphors is presented in Scheme 1. For comparison, pure $LaInO_3$:Sm^{3+} powders were produced in a similar process.

2.3. Characterization

X-ray power diffraction (XRD) was performed on a Rigaku-Dmax 2500 diffractometer using Cu Kα radiation (λ = 0.15405 nm). The accelerating voltage and emission current are 40 kV and 200 mA. Fourier transform IR spectra were performed on a Perkin-Elmer 580B IR spectrophotometer using KBr pellet technique. Field emission scanning electron microscope (FESEM) images were inspected on an S4800 (Hitachi) microscope equipped with an energy-dispersive X-ray spectrum (EDS, JEOL JXA-840). Transmission electron microscope (TEM) and high-resolution transmission electron microscope (HRTEM) images were carried out on a FEI Tecnai G^2 S-Twin with an acceleration voltage of 200 kV. The X-ray photoelectron spectra (XPS) were taken on a VG ESCALAB MK II electron energy spectrometer using Mg Kα (1253.6 eV) as the X-ray excitation source. A inductively coupled plasma (ICP-PLASMA 1000) was used to determine the actual doping of rare earth in the final products. The excitation and emission spectra were obtained on a Hitachi F-4500 spectrofluorimeter equipped with a 150 W xenon lamp as the excitation source. The cathodoluminescent (CL) measurements were carried out in an ultrahigh-vacuum chamber (10^{-8} Torr), where the phosphors were excited by an electron beam at a voltage range of 3–5 kV, and the spectra were recorded using an F-4500 spectrophotometer. Luminescence decay curves were obtained from a Lecroy Wave Runner 6100 Digital Oscilloscope (1 GHz) using a 250 nm laser (pulse width = 4 ns, gate = 50 ns) as the excitation source (Continuum Sunlite OPO). All the measurements were performed at room temperature.

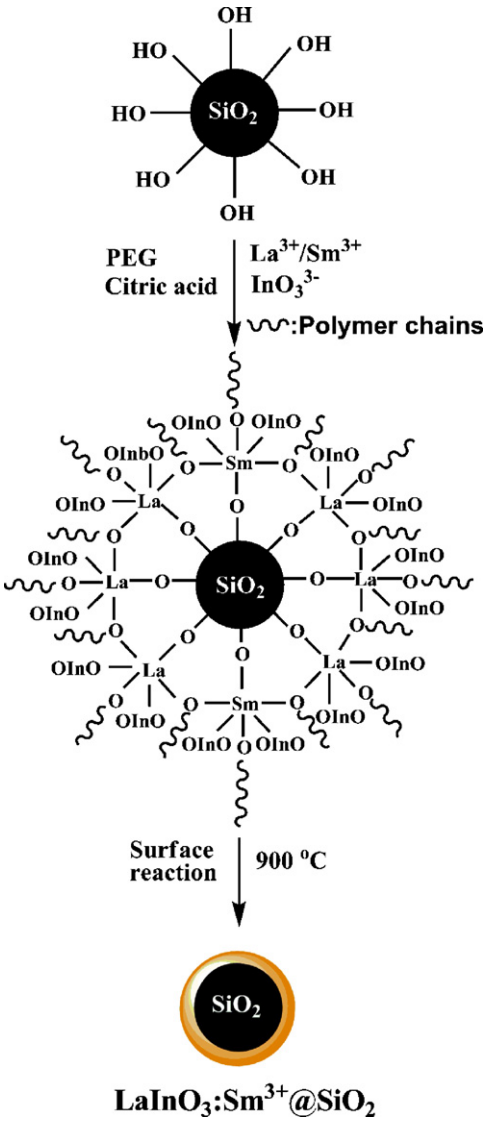

Scheme 1. Formation process of the core-shell structured $LaInO_3$:Sm^{3+}@SiO_2 particles.

3. Results and discussion

3.1. Phase identification and morphology

Fig. 1 shows the XRD patterns of pure SiO_2, $LaInO_3$:Sm^{3+}@SiO_2, and $LaInO_3$:Sm^{3+}, respectively. The vertical bars indicate the

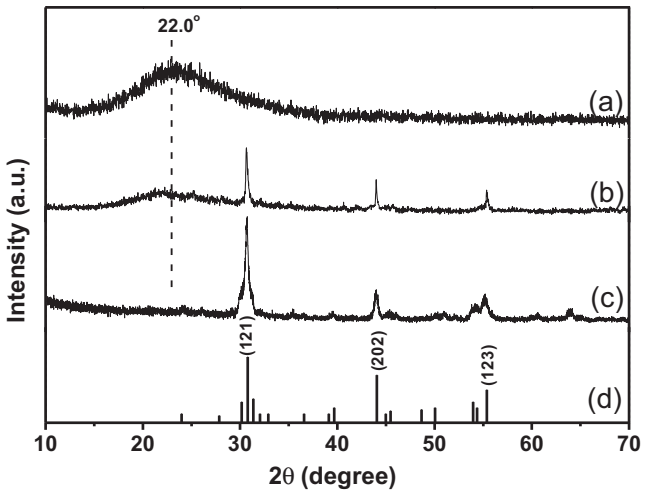

Fig. 1. X-ray diffraction patterns of pure SiO_2 $LaInO_3$:Sm^{3+}@SiO_2 (b), $LaInO_3$:Sm^{3+} (c), and the standard data for $LaInO_3$ (JCPDS No. 08-0148) (d).

standard bulk $LaInO_3$ peak positions (JCPDS No. 08–0148) for comparison. In Fig. 1a for pure silica, the broad band centered at $2\theta = 22^\circ$ can be assigned to the characteristic reflection from amorphous SiO_2 (JCPDS 29–0085). As for $LaInO_3$:Sm^{3+}@SiO_2 (Fig. 1b), the typical characteristic diffractions (observed at $2\theta = 30.77^\circ$, 44.07°, and 55.37°) suggest the crystalline phase of $LaInO_3$:Sm^{3+} on the surface of amorphous silica microspheres. The result is well consistent with the pure $LaInO_3$:Sm^{3+} powder (Fig. 1c). Furthermore, no second phase can be detected associated with the doped components, indicating that Sm^{3+} and Tb^{3+} can be completely incorporated into the host lattice of $LaInO_3$ due to the much similar ionic radii of the doped Ln^{3+} ($R_{Sm3+} = 1.08$ Å, $R_{Tb3+} = 1.18$ Å) to that of La^{3+} (1.18 Å), which can replace La^{3+} in $LaInO_3$:Ln^{3+} lattice. It should be noted that the crystallization temperature is low compared with the conventional solid-state reactions [46]. Because $La(NO_3)_3$ and $In(NO_3)_3$ can be homogeneously dispersed in the gel precursor at a molecular level that may promote the crystallinity of $LaInO_3$. The exact doping concentrations of Sm^{3+} in $LaInO_3$:Sm^{3+}@SiO_2 and Tb^{3+} in $LaInO_3$:Tb^{3+}@SiO_2 were determined to be 1.9 mol% and 5.1 mol% by ICP measurement, respectively.

FE-SEM images of pure SiO_2, $LaInO_3$:Sm^{3+}@SiO_2 microspheres, and bulk $LaInO_3$:Sm^{3+} powders are displayed in Fig. 2, respectively. The pure SiO_2 sample (Fig. 2a) consists of mono-dispersed uniform microspheres with a mean particle size of 300 nm. These particles are non-aggregated with narrow size distribution. In the case of $LaInO_3$:Sm^{3+}@SiO_2 microspheres (Fig. 2b), the morphological features, such as spherical, uniform microspheres, are still maintained, indicating that the coating of $LaInO_3$:Sm^{3+} phosphors have little effect on the basic morphological properties of pure SiO_2. Moreover, the small particles of bulk $LaInO_3$:Sm^{3+} particles (Fig. 2c) cannot be detected in the resulting $LaInO_3$:Sm^{3+}@SiO_2 sample, revealing the uniform coating of fluorescent layer on the surface of silica microspheres by our experimental process.

The typical TEM images of pure SiO_2, core-shell structured $LaInO_3$:Sm^{3+}@SiO_2 microspheres, and the HRTEM image of $LaInO_3$:Sm^{3+}@SiO_2 are shown in Fig. 3, respectively. As shown in Fig. 3a for pure silica, the TEM image gives the much identical morphological properties to that of SEM image (Fig. 2a), such as mono-dispersed, uniform, and non-aggregated spheres with very narrow size distribution. Moreover, the $LaInO_3$:Sm^{3+}@SiO_2 phos-

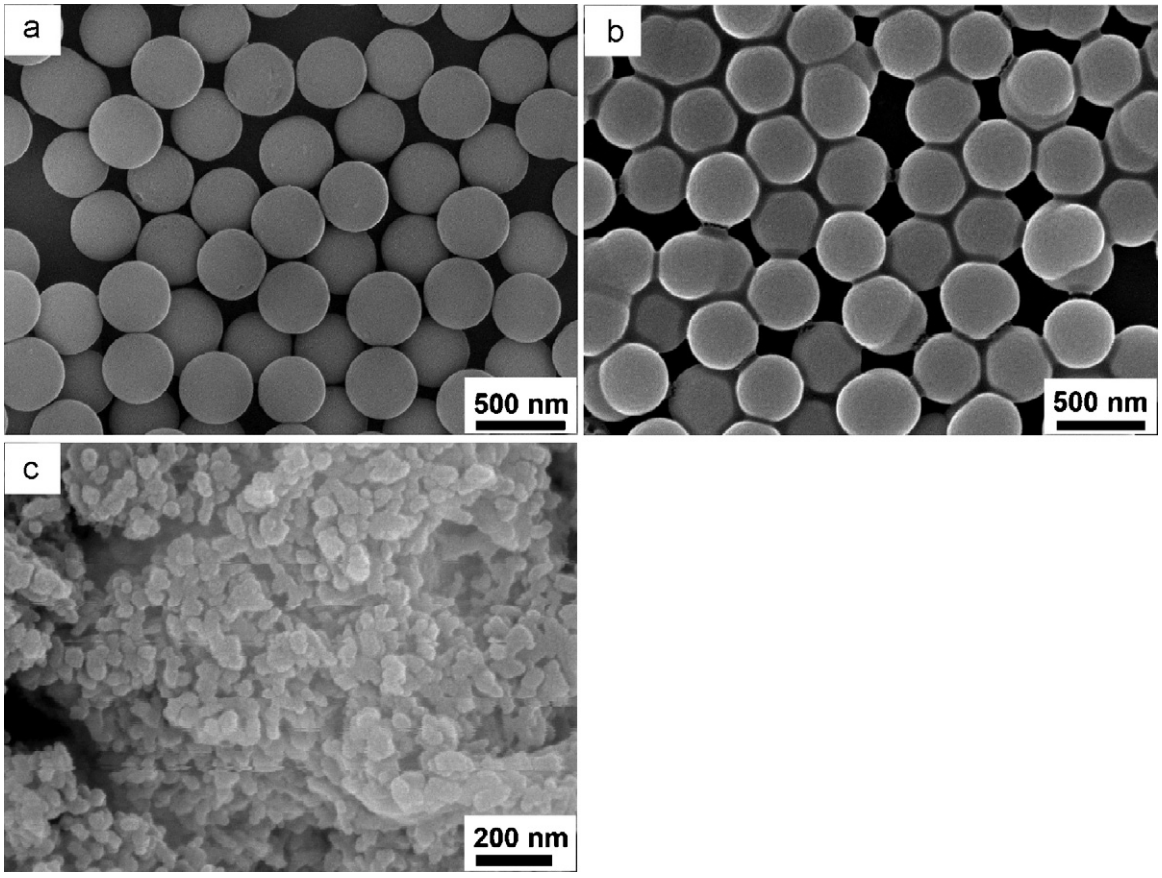

Fig. 2. SEM images of pure SiO_2 (a), $LaInO_3$:Sm^{3+}@SiO_2 (b), and bulk $LaInO_3$:Sm^{3+} powder (c).

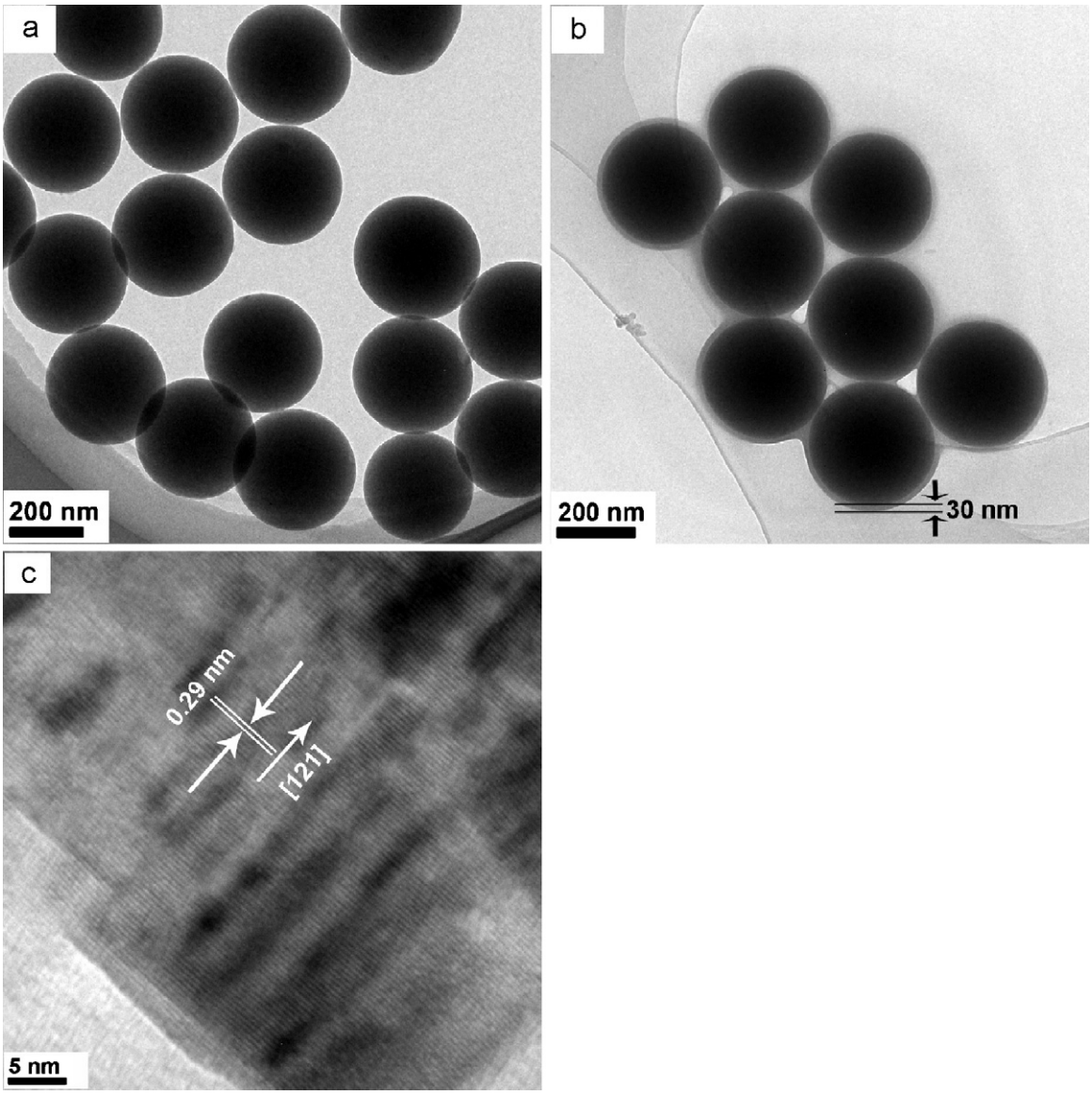

Fig. 3. TEM images of pure SiO_2 (a), $LaInO_3$:Sm^{3+}@SiO_2 (b), and HRTEM for $LaInO_3$:Sm^{3+}@SiO_2 coated with three times of phosphor layers (c).

phors (Fig. 3b) still maintain the morphological features of pure SiO_2 (Fig. 3a) except for a slightly larger particle size, which may be attributed to the coating of the $LaInO_3$:Sm^{3+} phosphors on the surface of silica core. It should be noted that an obvious core-shell structure can be detected due to the different electron penetrability between the core and shell. The cores consist of black spheres with an average size of 300 nm (pure silica spheres), and the shell exhibits gray color with a mean thickness of 30 nm. The HRTEM image (Fig. 3c) was obtained from the outer shell in the core-shell structured $LaInO_3$:Sm^{3+}@SiO_2 phosphors as marked in Fig. 3b. As shown, the lattice fringes related with the crystalline $LaInO_3$:Sm^{3+} are apparent, suggesting the high crystallinity of the sample. The lattice fringes of (1 2 1) planes with an interplanar distance of 0.29 nm are marked with arrows, which matches well with the *d* (1 2 1) spacing (0.2903 nm) of $LaInO_3$ (JCPDS No. 08–0148).

In the FT-IR spectra for the pure silica (Fig. 4a), the absorption bands assigned to OH (3431 cm^{-1}), H_2O (1631 cm^{-1}), Si–O–Si (υ_s, 1089 cm^{-1}; υ_{as}, 807 cm^{-1}), Si–OH (υ_s, 959 cm^{-1}), and Si–O (δ, 459 cm^{-1}) (where υ_s represents symmetric stretching, υ_{as} asymmetric stretching, and δ bending) can be detected [38,40]. It should be noted that the strong bands of OH (3431 cm^{-1})

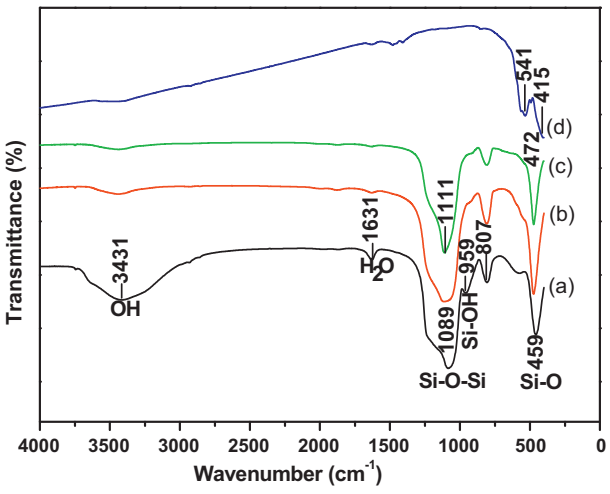

Fig. 4. FT-IR spectra for the 900 °C annealed pure SiO_2 (a), $LaInO_3$:Sm^{3+}@SiO_2 (b), $LaInO_3$:Tb^{3+}@SiO_2 (c), and pure $LaInO_3$:Sm^{3+} powder (d).

and H_2O (1631 cm^{-1}) suggest that a large number of OH groups and H_2O molecules exist on the surface of silica, which play a key role in bonding metal ions from the coating sol, thus forming the phosphor coating on the silica surfaces in the following heating process, as shown in Scheme 1. Seen from the IR spectrum for pure $LaInO_3:Sm^{3+}$ powders (Fig. 4d), an absorption peak at 541 cm^{-1} and a weak one at 415 cm^{-1} can be associated the stretching vibrations of the InO_6 octahedra [50]. As for the core-shell structured $LaInO_3:Sm^{3+}@SiO_2$ product (Fig. 4b) and $LaInO_3:Tb^{3+}@SiO_2$ product (Fig. 4c), the absorption peaks of Si–O (472 cm^{-1}) and Si–O–Si bond (809 cm^{-1}, 1111 cm^{-1}) assigned to silica are observed, and the peaks of InO_6 octahedra in $LaInO_3:Sm^{3+}$ disappears, which may be covered by the bending vibration of Si–O bond at 472 cm^{-1}. The peaks of OH groups almost disappear for the 900 °C annealed $LaInO_3:Sm^{3+}@SiO_2$ core-shell structured phosphors.

XPS has been known as a useful tool for determining the surface component and composition of a product. The survey and the respective element XPS spectra of $LaInO_3:Sm^{3+}@SiO_2$ are given in Fig. 5. The binging energy of Sm (3d, 1088 eV), In ($3d_{3/2}$, 451.6 eV) ($3d_{5/2}$, 443.9 eV), La ($3d_{3/2}$, 855.1 eV) ($3d_{5/2}$, 838.7 eV), Si (2p, 103.5 eV) and O (1s, 531.9 eV) are apparent. By combination of the XRD and FT-IR analysis, it can be deduced that these signals are assigned to $LaInO_3$ shell and silica core. XPS result provides additional evidence for the coating of $LaInO_3$ phosphors on the silica spheres.

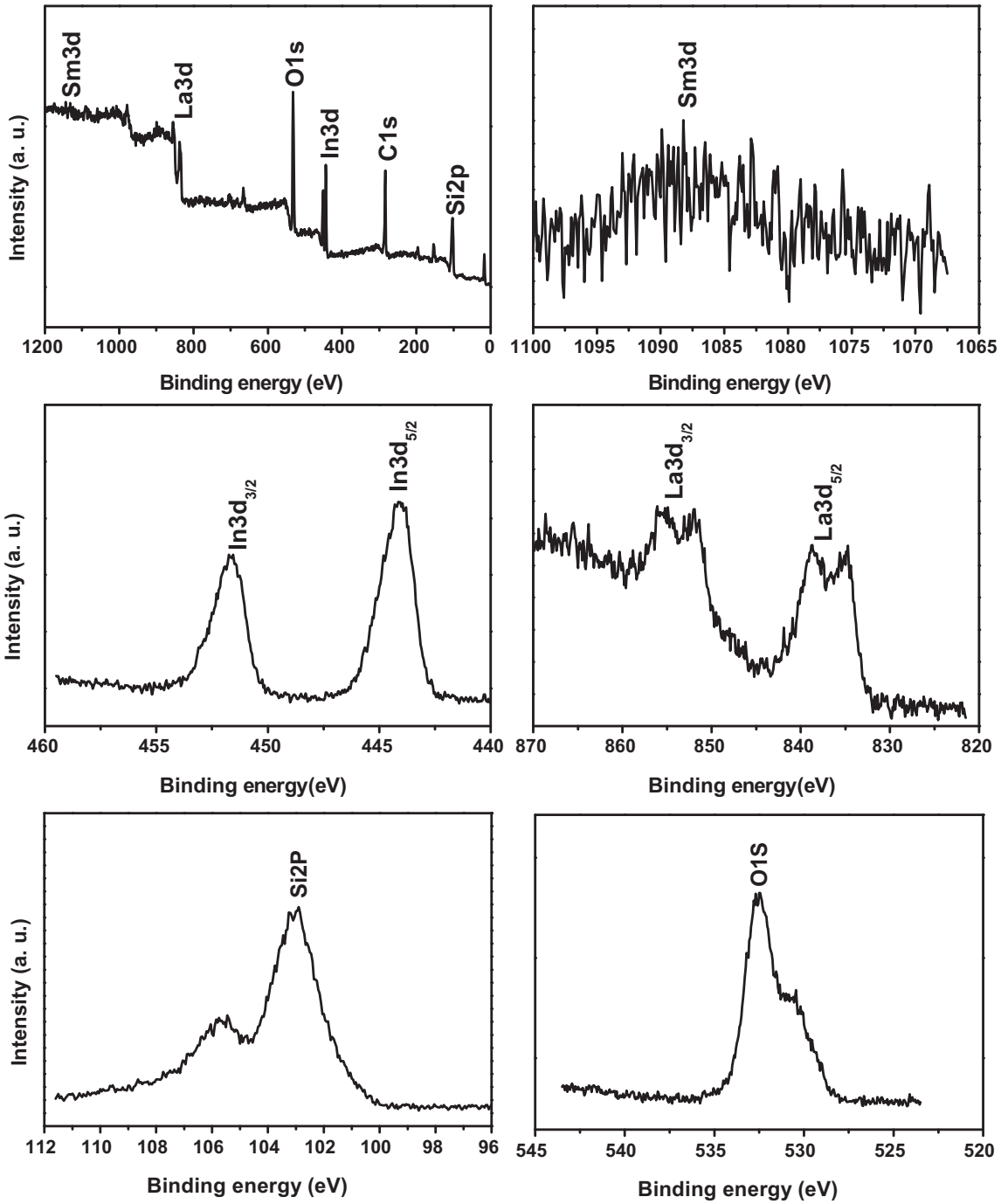

Fig. 5. The survey and the respective element XPS of $LaInO_3:Sm^{3+}@SiO_2$.

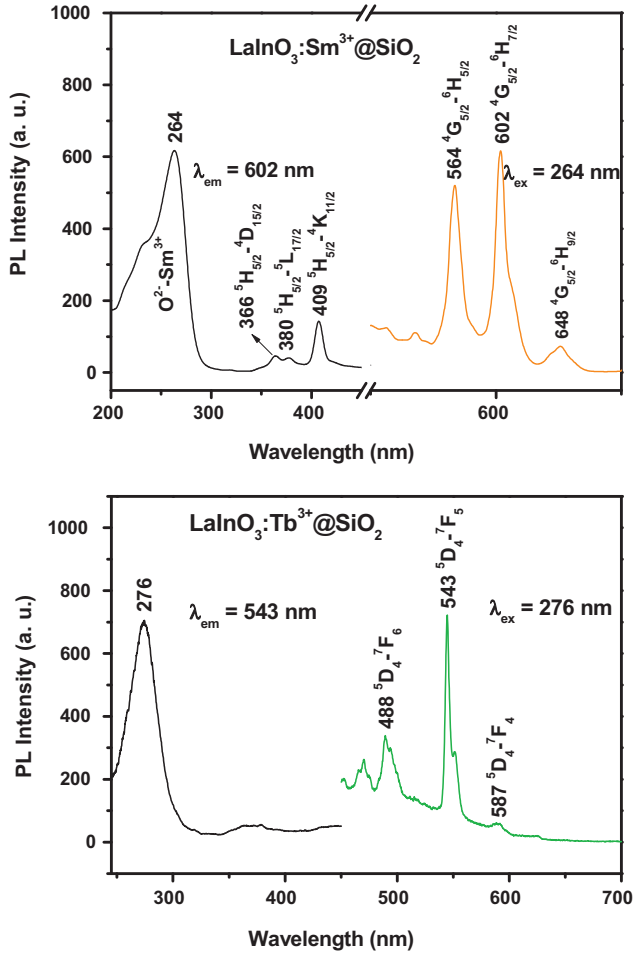

Fig. 6. Excitation (left) and emission spectra (right) of $LaInO_3:Sm^{3+}@SiO_2$ (a) and $LaInO_3:Tb^{3+}@SiO_2$ (b). (For interpretation of the references to color in this figure legend, the reader is referred to the web version of the article.)

3.2. Luminescent properties

The PL properties of core-shell structured $LaInO_3:Sm^{3+}@SiO_2$ phosphors were characterized by excitation and emission spectra, as shown in Fig. 6a. The excitation spectrum (Fig. 6a, left) monitored with 602 nm emission of Sm^{3+} ($^4G_{5/2}$–$^5H_{7/2}$) consists of a broad band with a maximum at 264 nm and some weak peaks at 366, 380 and 409 nm. The broad band can be attributed to the oxygen (2p)-to-samarium (4f) (Sm^{3+}–O^{2-}) charge transfer transition [51]. And the weak lines can be associated with the transitions from the ground $^6H_{5/2}$ level to $^4D_{15/2}$ (366 nm), $^4L_{17/2}$ (380 nm), and $^4K_{11/2}$ (409 nm) [52]. Excitation at 264 nm yields the characteristic emissions of the Sm^{3+} ions at 564 nm ($^4G_{5/2}$–$^6H_{5/2}$), 602 nm ($^4G_{5/2}$–$^6H_{7/2}$), and 648 nm ($^4G_{5/2}$–$^6H_{9/2}$). It is obvious that the emission spectrum is dominated by the $^4G_{5/2}$–$^6H_{5/2}$ and $^4G_{5/2}$–$^6H_{7/2}$ transitions of Sm^{3+}. Under excitation of short ultraviolet, the core-shell structured $LaInO_3:Tb^{3+}@SiO_2$ phosphors exhibit a green luminescence. The excitation and emission spectra of $LaInO_3:Tb^{3+}@SiO_2$ phosphors are given in Fig. 6b. Monitored by the emission of the Tb^{3+} ($^5D_4$–$^7F_5$) transition at 543 nm, the obtained excitation spectrum (Fig. 6b, left) includes a broad excitation band with a maximum at 276 nm and a weak broad peak beyond 350 nm, which can be assigned to the $4f^8$–$4f^7$ 5d transitions of Tb^{3+} and the f–f transitions within the Tb^{3+} $4f^8$ configuration, respectively. Upon excitation at the $4f^8$–$4f^7$ 5d transition at 276 nm, the emission spectrum (Fig. 6b, right) is composed of characteristic f–f transition lines within $4f^8$ electron configuration, such as $^5D_4$–$^7F_6$ (488 nm) in the blue region, $^5D_4$–$^7F_5$ (543 nm) in the green region, and $^5D_4$–$^7F_4$ (587 nm) in the red region, respectively. It is obvious that the $^5D_4$–$^7F_5$ green emission (543 nm) is the most prominent group. It should be noted that no apparently blue emissions of $^5D_3$–^7F_J transitions can be detected which may be caused by the cross-relaxation between $^5D_3$–$^5D_4$ and $^7F_0$–$^7F_6$ of two neighboring Tb^{3+} ions [40,52].

The respective luminescence decay curve of the core-shell structured $LaInO_3:Sm^{3+}@SiO_2$ and $LaInO_3:Tb^{3+}@SiO_2$ phosphors treated at 900 °C is presented in Fig. 7. It can be seen that two luminescence decay curves of Sm^{3+} ($^4G_{5/2}$–$^6H_{7/2}$, 602 nm) in $LaInO_3:Sm^{3+}@SiO_2$ and Tb^{3+} ($^5D_4$–$^7F_5$, 543 nm) in $LaInO_3:Tb^{3+}@SiO_2$ can all be well fitted to single exponential functions, which can be associated with the homogenous environment of the activator ions (one kind of emission center in the host lattice). And the lifetimes of Sm^{3+} ($^4G_{5/2}$) and Tb^{3+} ($^5D_4$) in $LaInO_3:Ln^{3+}@SiO_2$ phosphors were determined to be 0.67 ms and 0.49 ms, respectively, which are basically in the same order (ms) of magnitude as the reported bulk phosphors [44].

The core-shell structured $LaInO_3:Sm^{3+}@SiO_2$ and $LaInO_3:Tb^{3+}@SiO_2$ phosphors show respective orange–red and green emission upon excitation by the low voltage electron beam. It can be seen that the typical emission spectrum of the core-shell $LaInO_3:Sm^{3+}@SiO_2$ phosphors (Fig. 8a) are nearly identical to the PL emission (Fig. 6a, right) except for a lower intensity under the excitation with the accelerating voltage of 5 kV and filament current of 105 mA. Fig. 8b exhibits the intensities of the CL emission

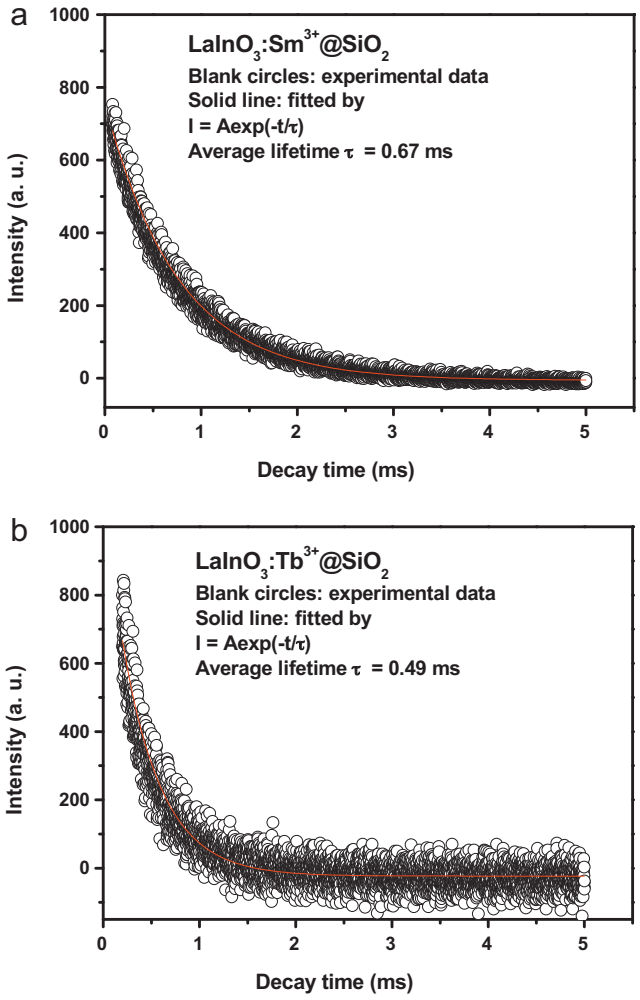

Fig. 7. Decay curves for the luminescence of Sm^{3+} in $LaInO_3:Sm^{3+}@SiO_2$ (a) and Tb^{3+} in $LaInO_3:Tb^{3+}@SiO_2$ (b).

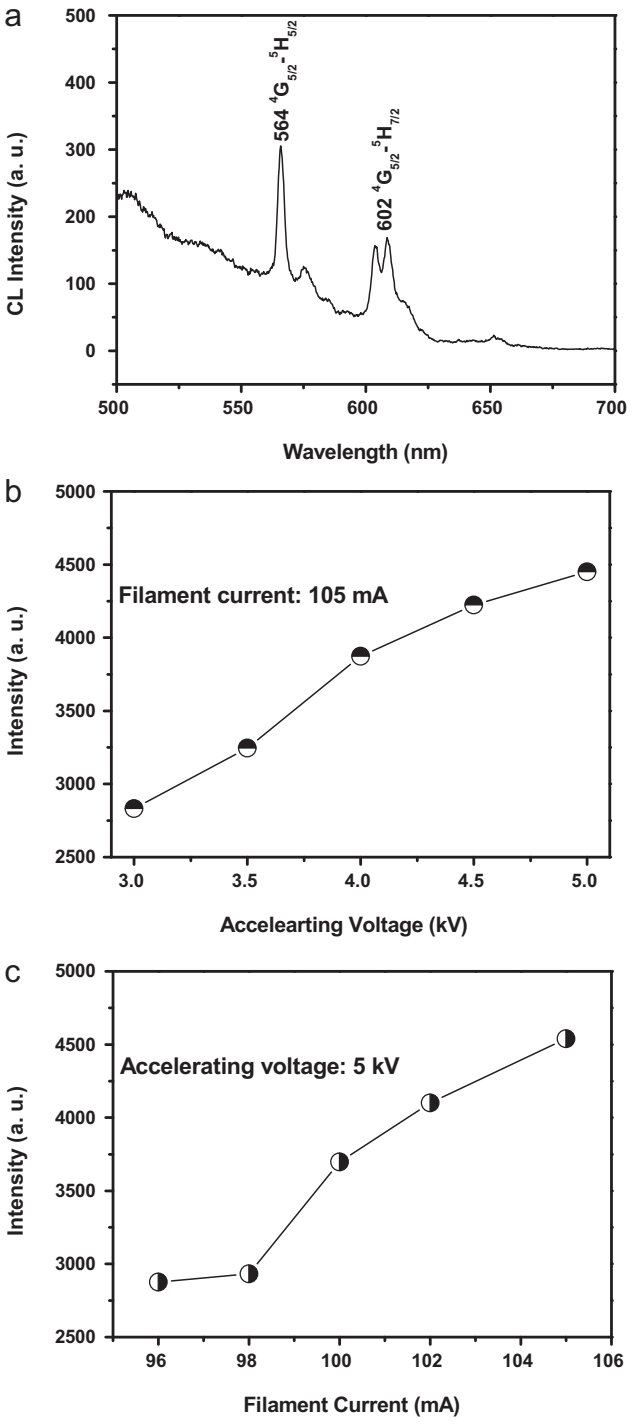

Fig. 8. The CL spectrum of $LaInO_3$:Sm^{3+}@SiO_2 (a) and the CL intensities of Sm^{3+} in $LaInO_3$:Sm^{3+}@SiO_2 as a function of accelerating voltage (b) and filament current (c).

for the core-shell structured $LaInO_3$:Sm^{3+}@SiO_2 as a function of the accelerating voltage from 3.0 to 5.0 kV when the filament current is fixed at 105 mA. Obviously, the emission intensity increases with the accelerating voltage, which can be due to the deeper penetration of electrons into the phosphors by the larger electron beam current density. When the accelerating voltage is fixed at 5 kV, the CL intensity shows the similar increasing trend with the filament current from 96 to 105 mA (Fig. 8c). The electron penetration depth can be estimated by the empirical formula: L [Å] = $250(A/\rho)(E/Z^{1/2})^n$, where $n = 1.2/(1 - 0.29 \log Z)$, A is the atomic weight, ρ is the density, Z is the atomic number, and E is the accelerating voltage (kV) [53]. Thus, either the increase of the accelerating voltage or the filament current can bring deeper penetration of electrons into the phosphor's body. In accordance, more plasma will be produced, resulting in more Ln^{3+} ions are excited, the cathodoluminescent intensity is therefore increased. The CL properties and the intensities as functions of the accelerating voltage and the filament current for the core-shell structured $LaInO_3$:Tb^{3+}@SiO_2 are given in Fig. 9. Much similar results are obtained to those of $LaInO_3$:Sm^{3+}@SiO_2 phosphors.

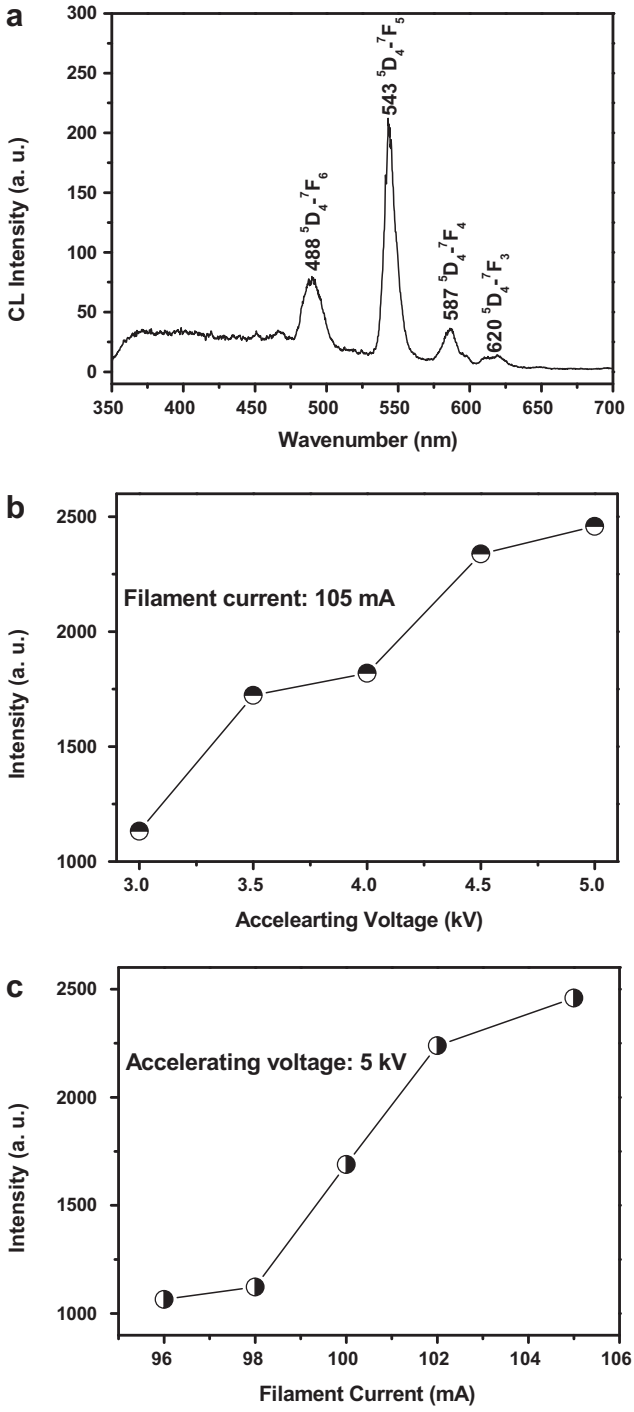

Fig. 9. The CL spectrum of $LaInO_3$:Tb^{3+}@SiO_2 (a) and the CL intensities of Tb^{3+} in $LaInO_3$:Tb^{3+}@SiO_2 as a function of accelerating voltage (b) and filament current (c).

4. Conclusions

A facile and low-cost sol–gel process has been developed to deposit a uniform $LaInO_3:Sm^{3+}$ and $LaInO_3:Tb^{3+}$ layers on the surfaces of SiO_2 microspheres. The realized core-shell structured $LaInO_3:Ln^{3+}@SiO_2$ phosphors keep the spherical shape of the pure silica spheres except for a coating layer of crystalline $LaInO_3:Ln^{3+}$ with the thickness of 30 nm. Under UV light or low–voltage electron beam excitation, the core-shell structured $LaInO_3:Sm^{3+}$ and $LaInO_3:Tb^{3+}$ phosphors exhibit the characteristic emissions of Sm^{3+} and Tb^{3+}, which are much similar to those of the corresponding bulk $LaInO_3:Ln^{3+}$ phosphors. Due to the spherical morphology, uniform particle size, and diverse fluorescent properties, this kind of core-shell structured materials are of special interest in FEDs applications.

Acknowledgements

This project is financially supported by National Basic Research Program of China (2007CB935502), the National Natural Science Foundation of China (NSFC 20871035, 50702057, 50872131, 00610227), China Postdoctoral Special Science Foundation (200808281), and Harbin Sci.-Tech. Innovation Foundation (No. 2009RFQXG045).

References

[1] Y.F. Zhu, H.G. Pan, M.X. Gao, J.X. Ma, Y.Q. Lei, Q.D. Wang, Int. J. Hydrogen Energy 28 (2003) 311.
[2] H.G. Pan, R. Li, Y.F. Liu, M.X. Gao, H. Miao, Y.Q. Lei, Q.D. Wang, J. Alloys Compd. 463 (2008) 189.
[3] Y.F. Liu, K. Luo, Y.F. Zhou, M.X. Gao, H.G. Pan, J. Alloys Compd. 481 (2009) 473.
[4] M. Gao, H. Miao, Y. Zhao, Y.F. Liu, H.G. Pan, J. Alloys Compd. 484 (2009) 249.
[5] J.H. Wang, J.J. Hu, Y.F. Liu, Z.T. Xiong, G.T. Wu, H.G. Pan, P. Chen, J. Mater. Chem. 19 (2009) 2141.
[6] H.G. Pan, F.M. Yang, C.P. Chen, N. Tang, X.F. Han, Q.D. Wang, J. Magn. Magn. Mater. 163 (1996) 221.
[7] L.X. Chen, Y.Q. Lei, G.M. Zhu, H.G. Pan, K. Ren, Z.Z. Li, X.G. Yang, Q.D. Wang, J. Alloys Compd. 293–295 (1999) 684.
[8] B. Kotur, O. Myakush, H. Michor, E. Bauer, J. Alloys Compd. 299 (2010) 135.
[9] X.D. Feng, D.C. Sayle, Z.L. Wang, M.S. Paras, B. Santora, A.C. Sutorik, T.X.T. Sayle, Y. Yang, Y. Ding, X.D. Wang, Y.S. Her, Science 312 (2006) 1504.
[10] Y.A. Yang, O. Chen, A. Angerhofer, Y.C. Cao, J. Am. Chem. Soc. 128 (2006) 12428.
[11] G. Blasse, B.C. Grabmaier, Springer-Verlag, Berlin, Heidelberg, 1994.
[12] F. Wang, Y. Han, C.S. Lim, Y.H. Lu, J. Wang, J. Xu, H.Y. Chen, C. Zhang, M.H. Hong, X.G. Liu, Nature 463 (2010) 1061.
[13] T. Justel, H. Nikol, C. Ronda, Angew. Chem. Int. Ed. 37 (1998) 3085.
[14] F. Auzel, Chem. Rev. 104 (2004) 139.
[15] E. Downing, L. Hesselink, J. Ralston, R. Macfarlane, Science 273 (1996) 1185.
[16] X. Wang, J. Zhuang, Q. Peng, Y.D. Li, Nature 437 (2005) 121.
[17] R. Si, Y.W. Zhang, L.P. You, C.H. Yan, Angew. Chem. Int. Ed. 44 (2005) 3256.
[18] K. Kompe, H. Borchert, J. Storz, A. Lobo, S. Adam, T. Moller, M. Haase, Angew. Chem. Int. Ed. 42 (2003) 5513.
[19] T. Yu, J. Joo, Y.I. Park, T. Hyeon, J. Am. Chem. Soc. 128 (2006) 1786.
[20] J.W. Stouwdam, F. van Veggel, Nano Lett. 2 (2002) 733.
[21] B. Pastoriza-Santos, B. Scholer, F. Caruso, Adv. Funct. Mater. 11 (2001) 122.
[22] G.X. Wang, H.M. Wu, D. Wexler, H.K. Liu, O. Savadogo, J. Alloys Compd. 503 (2010) L1.
[23] S.Y. Tan, P.P. Yang, N. Niu, S.L. Gai, J. Wang, X.Y. Jing, J. Lin, J. Alloys Compd. 490 (2010) 684.
[24] L.M. Liz-Marzán, M. Giersig, P. Mulvaney, Langmuir 12 (1996) 4329.
[25] H.B. Hu, Z.H. Wang, L. Pan, J. Alloys Compd. 492 (2010) 656.
[26] F. Caruso, R.A. Caruso, H. Mohwald, Science 282 (1998) 1111.
[27] F. Caruso, H. Lichtenfeld, M. Giersig, H. Mohwald, J. Am. Chem. Soc. 120 (1998) 8523.
[28] R.A. Caruso, J.H. Schattka, A. Greiner, Adv. Mater. 13 (2001) 1577.
[29] M. Giersig, T. Ung, L.M. LizMarzan, P. Mulvaney, Adv. Mater. 9 (1997) 570.
[30] M. Ocana, W.P. Hsu, E. Matijevic, Langmuir 7 (1991) 2911.
[31] W.P. Hsu, R.C. Yu, E. Matijevic, J. Colloid Interface Sci. 156 (1993) 56.
[32] H. Giesche, E. Matijevic, J. Mater. Res. 9 (1994) 436.
[33] V. Salgueirino-Maceira, M. Spasova, M. Farle, Adv. Funct. Mater. 15 (2005) 1036.
[34] A. Dokoutchaev, J.T. James, S.C. Koene, S. Pathak, G.K.S. Prakash, M.E. Thompson, Chem. Mater. 11 (1999) 2389.
[35] R.A. Caruso, M. Antonietti, Chem. Mater. 13 (2001) 3272.
[36] K.W. Chang, J.J. Wu, Adv. Mater. 17 (2005) 241.
[37] C.K. Lin, Y.Y. Li, M. Yu, P.P. Yang, J. Lin, Adv. Funct. Mater. 17 (2007) 1459.
[38] M. Yu, J. Lin, J. Fang, Chem. Mater. 17 (2005) 1783.
[39] M. Yu, H. Wang, C.K. Lin, G.Z. Li, J. Lin, Nanotechnology 17 (2006) 3245.
[40] M. Yu, J. Lin, J. Fu, H.J. Zhang, Y.C. Han, J. Mater. Chem. 13 (2003) 1413.
[41] H. Wang, C.K. Lin, X.M. Liu, J. Lin, M. Yu, Appl. Phys. Lett. 87 (2005).
[42] P.Y. Jia, X.M. Liu, G.Z. Li, M. Yu, J. Fang, J. Lin, Nanotechnology 17 (2006) 734.
[43] D.B. Rogers, J.M. Honig, J.B. Goodenough, Mater. Res. Bull. 2 (1967) 223.
[44] X.M. Liu, J. Lin, Solid State Sci. 11 (2009) 2030.
[45] X.M. Liu, L.S. Yan, J. Lin, J. Electrochem. Soc. 156 (2009) P1.
[46] N. Lakshminarasimhan, U.V. Varadaraju, Mater. Res. Bull. 41 (2006) 724.
[47] H. He, X. Huang, L. Chen, Solid State Ionics 130 (2000) 183.
[48] W. Stöber, A. Fink, E. Bohn, J. Colloid Interface Sci. 26 (1968) 62.
[49] M.P. Pechini, US Patent 3330697, 1967.
[50] A. Baszczuk, M. Jasiorski, M. Nyk, J. Hanuza, M. Mączka, W. Stręk, J. Alloys Compd. 394 (2005) 88.
[51] T.R.N. Kutty, A. Nag, J. Mater. Chem. 13 (2003) 2271.
[52] G. Blasse, B.C. Grabmaier, Luminescent Materials. Springer-Verlag, Berlin, Heidelbery, 1994 (Chapters 4 and 5).
[53] C. Feldman, Phys. Rev. 117 (1960) 455.